RESEARCH ARTICLE | FEBRUARY 03 2023

On the synthesis and characterization of bimagnetic CoO/NiFe₂O₄ heterostructured nanoparticles

Muhammad S. Uddin **≥** ; Robert A. Mayanovic ; Mourad Benamara



AIP Advances 13, 025314 (2023) https://doi.org/10.1063/9.0000561





CrossMark

Articles You May Be Interested In

Bimagnetic nanoparticles with enhanced exchange coupling and energy products

Journal of Applied Physics (January 2009)

Core-shell FeNi-Ni_xFe_{3-x}O₄ nanowires

Journal of Vacuum Science & Technology B (July 2015)

Magnetic and electronic properties of bimagnetic materials comprising cobalt particles within hollow silica decorated with magnetite nanoparticles

Journal of Applied Physics (September 2013)

AIP Advances
Fluids and Plasmas Collection



On the synthesis and characterization of bimagnetic CoO/NiFe₂O₄ heterostructured nanoparticles

Cite as: AIP Advances 13, 025314 (2023); doi: 10.1063/9.0000561 Submitted: 3 October 2022 • Accepted: 18 November 2022 • Published Online: 3 February 2023











Muhammad S. Uddin, 1, 10 Robert A. Mayanovic, 10 and Mourad Benamara 20



AFFILIATIONS

- Department of Physics, Astronomy and Materials Science, Missouri State University, Springfield, Missouri 65897, USA
- ²University of Arkansas, Fayetteville, Arkansas 72701, USA

Note: This paper was presented at the 67th Annual Conference on Magnetism and Magnetic Materials.

a) Author to whom correspondence should be addressed: sharif0162@gmail.com

ABSTRACT

Bimagnetic nanoparticles show promise for applications in energy efficient magnetic storage media and magnetic device applications. The magnetic properties, including the exchange bias of nanostructured materials can be tuned by variation of the size, composition, and morphology of the core vs overlayer of the nanoparticles (NPs). The purpose of this study is to investigate the optimal synthesis routes, structure and magnetic properties of novel CoO/NiFe₂O₄ heterostructured nanocrystals (HNCs). In this work, we aim to examine how the size impacts the exchange bias, coercivity and other magnetic properties of the CoO/NiFe₂O₄ HNCs. The nanoparticles with sizes ranging from 10 nm to 24 nm were formed by synthesis of an antiferromagnetic (AFM) CoO core and deposition of a ferrimagnetic (FiM) NiFe₂O₄ overlayer. A highly crystalline magnetic phase is more likely to occur when the morphology of the core-overgrowth is present, which enhances the coupling at the AFM-FiM interface. The CoO core NPs are prepared using thermal decomposition of Co(OH)2 at 600 °C for 2 hours in a pure argon atmosphere, whereas the HNCs are obtained first using thermal evaporation followed by hydrothermal synthesis. The structural and morphological characterization made using X-ray diffraction (XRD), high-resolution transmission electron microscopy (HR-TEM), and scanning electron microscopy (SEM) techniques verifies that the HNCs are comprised of a CoO core and a NiFe₂O₄ overgrowth phase. Rietveld refinement of the XRD data shows that the CoO core has the rocksalt (Fd3 m) crystal structure and the NiFe₂O₄ overgrowth has the spinel (C12/m1) crystal structure. SEM-EDS data indicates the presence and uniform distribution of Co, Ni and Fe in the HNCs. The results from PPMS magnetization measurements of the CoO/NiFe₂O₄ HNCs are discussed herein.

© 2023 Author(s). All article content, except where otherwise noted, is licensed under a Creative Commons Attribution (CC BY) license (http://creativecommons.org/licenses/by/4.0/). https://doi.org/10.1063/9.0000561

I. INTRODUCTION

Nanoscale heterostructures of magnetically active materials exhibit intriguing properties that can be of great importance in spintronic devices, catalysis, materials chemistry, magnetic recording media, magnetic resonance imaging, drug delivery, and hyperthermia. 1-3 Transition metal oxides having different structure and/or composition that are incorporated in the heterostructure have been shown to offer very interesting coupling effects, such as obtaining magnetoelectric/multiferroic properties using strain or an exchange bias (EB) effect.⁴ It is extremely desirable to tune spin structures at antiferromagnetic (AFM) surfaces⁵ and interfaces

not only for these developing technologies but also to obtain a new understanding of the underlying magnetic processes.^{6–8} The inclusion of an AFM component in magnetic heterostructured nanocrystals (HNCs), such as CoO, Cr2O3, MnO, or NiO, is particularly advantageous when paired with a ferro/ferrimagnetic (FM/FiM) component because it enhances the system's effective magnetic anisotropy through interface exchange coupling. Achieving stable magnetic anisotropic energies in nanoparticulate heterostructures may necessitate the modification of their properties since the magnetic anisotropy of nanomaterials is strongly reliant on the crystalline structure, size, shape, interface quality, and composition. 10-14 Consequently, the development of more advanced magnetic nanoparticles made of two (or more) materials, such as core/overlayer heterostructures, has been facilitated by breakthroughs in synthetic chemistry that enable unprecedented control over growth conditions.¹⁵ The study of bi-magnetic core/overlayer magnetic nanoparticles, in which both the core and the overlayer exhibit magnetic properties [ferromagnetic (FM), ferrimagnetic (FiM), or antiferromagnetic (AFM)], is a particularly interesting topic in core/overlayer magnetic heterostructured nanoparticle research.¹⁰ When the morphology of the core-overgrowth is present, a highly crystalline magnetic phase is more likely to form for closely matched crystalline components, which increases the coupling at the AFM-FiM interface. Although different core/overlayer phase combinations (spinel-spinel, spinel-rock salt) have been studied, herein, we report on the synthesis, structure, and magnetic properties of novel CoO/NiFe2O4 heterostructures which contain bimetallic spinel overgrowths.

II. EXPERIMENTAL METHODS

The synthesis of the HNCs involved three steps. For the preparation of CoO nanoparticles, the process outlined by El Kemary et al. 16 is followed which involves thermal decomposition of Co(OH)₂ to generate CoO precursors. First, absolute ethanol was used to dissolve cobalt chloride hexahydrate (0.11M) as a precursor and was added to a solution of hydrazine monohydrate, and sodium hydroxide. The ratio of CoCl₂·6H₂O to N₂H₄·H₂O and NaOH was kept at 1:5:10. Following that, the solution was stirred well with a magnetic stirrer and dried for 2 hours at 600 °C in an oven under pure argon atmosphere. The resulting powdered CoO was then washed with water that has been deionized (DI) and then centrifuged to remove residues and excess water. The NiFe₂O₄ phases were then grown over the CoO core partly using our hydrothermal nanophase epitaxy method. 16,17 First, following a 15-20 minute N₂ purging of HPLC graded water ($p^H = 7$) at 70-80 °C to remove O₂, 0.10 g $Ni(N0_3)_2 \cdot 6H_2O$ and 0.25 g $Fe(N0_3)_3 \cdot 9H_2O$ were added to the deoxygenated water and sonicated for ~20 minutes. Subsequently, 0.11 g of CoO nanoparticles were added to the solution, which underwent a 30 minute sonication. The mixture was then transferred to a 250 ml flask in a rotary evaporator, wherein the evaporation was made at 80-90 °C and reduced pressure for about 3 hours. The suspension from the flask was then transferred to an autoclave and hydrothermally treated at 200 °C for 12 hours. Following the completion of the hydrothermal synthesis, the product was rinsed with DI water, centrifuged, and then dried at a temperature of ~ 50 °C.

The samples were subjected to XRD analysis using a Bruker D8 Discover diffractometer that was operated at 40 kV and 40 mA with a 0.6 mm slit and a Cu K- α X-ray source with a wavelength of $\lambda=1.541$ 84 Å. Using the Rietveld method, TOPAS software was used to refine all XRD patterns. A JEOL SEM operating at 2 kV and 5 mm WD was used to carry out the SEM imaging characterization. Carbon tape was used to mount the samples for SEM imaging. A SEM-EDS (Oxford Instruments) and a field emission gun were used to perform a preliminary elemental analysis. The TEM imaging and EELS mapping of the samples were performed on an FEI Titan 80–300 instrument at the University of Arkansas Nano-Bio Materials Characterization Facility, with the field emission gun set to 300 keV. The magnetization data from the samples were measured utilizing a Quantum Design Physical Property Measurement

System (PPMS) at CCMR, Cornell University. For the magnetization vs temperature data, the samples were first cooled to 5 K from room temperature for both the field-cooled (FC) and zero-field-cooled (ZFC) measurements. Additionally, for the FC measurements, each sample was cooled in a field of 50 Oe, whereas the magnetization data were acquired in an external field of 50 Oe. The FC and ZFC hysteresis curves were measured from $-25\,000$ Oe to $+25\,000$ Oe, and at 5 K and 300 K.

III. RESULTS AND DISCUSSION

The designations and size of the HNC samples reported on this study are shown in Table I. The powder x-ray diffraction pattern measured from HNC1 at room temperature is shown in Fig. 1(a). XRD analysis shows that, the CoO core of the HNC1 sample has the rocksalt structure with space group Fd3m, the NiFe₂O₄ overgrowth has the spinel structure with space group of C12/m1, and there is a minor contribution from a cubic phase having the F43m space group. The minor phase corresponds to nanocrystalline Co₃O₄. When compared to the typical ratio of peak intensities for bulk CoO, the (111) peak's higher intensity (at 36.76°) implies that the nanocrystalline structures may be somewhat preferentially orientated within the powder sample. To further examine their structural characteristics, the XRD data obtained from the HNC1 sample were refined using the Rietveld method. For the CoO core and NiFe₂O₄ overgrowth phase (Fd3m) and (C12/m1) structure CIF files were used along with an (F43m) structure CIF file for the impurity phase, in the refining of the XRD spectra. The fit using the Rietveld method is depicted in Fig. 1(b) and confirms that there is 67.21 at. % of the CoO core, 27.86 at. % of the NiFe₂O₄ overgrowth, and 4.93 at. % of the Co₃O₄ in the HNC1 sample. Due to Ni and Fe doping in the overgrowth region, it was observed that the lattice parameters and unit cell volume were slightly increased for the NiFe₂O₄ as compared to CoO, which is in line with the difference in ionic radii between Ni^{2+} , Co^{2+} , and Fe^{2+} .

The XRD analysis of the remainder of the HNC samples was consistent with the analysis described above except for the absence of the ${\rm Co_3O_4}$ phase in the other two samples. The structure of the overgrowth is directly affected due to the incorporation of Ni and Fe and the resulting formation of the bi-metallic oxide phase. Furthermore, the formation of such an overgrowth can have a direct impact upon the magnetic characteristics of HNCs. The crystallite size of the samples was estimated from the XRD data using the Scherrer equation within fitting in TOPAS, which range between 10 and 24 nm (see Table I).

Figure 1(c) shows an SEM image of the agglomerated nanoparticles in the HNC1 sample. The corresponding SEM-EDS data reveal

TABLE I. Saturation magnetization (M_S), remanent magnetization (M_R), coercivity (H_C), exchange bias field (H_F) of HNCs at 5 K

Sample	HNC1	HNC2	HNC3
M _S (emu/g)	24.6	10.4	8.3
M _R (emu/g)	19.8	9.1	7.9
H _C (Oe)	7412	6052	9624
H _E (Oe)	168	520	632
Size (nm)	14.8	18.1	12.5

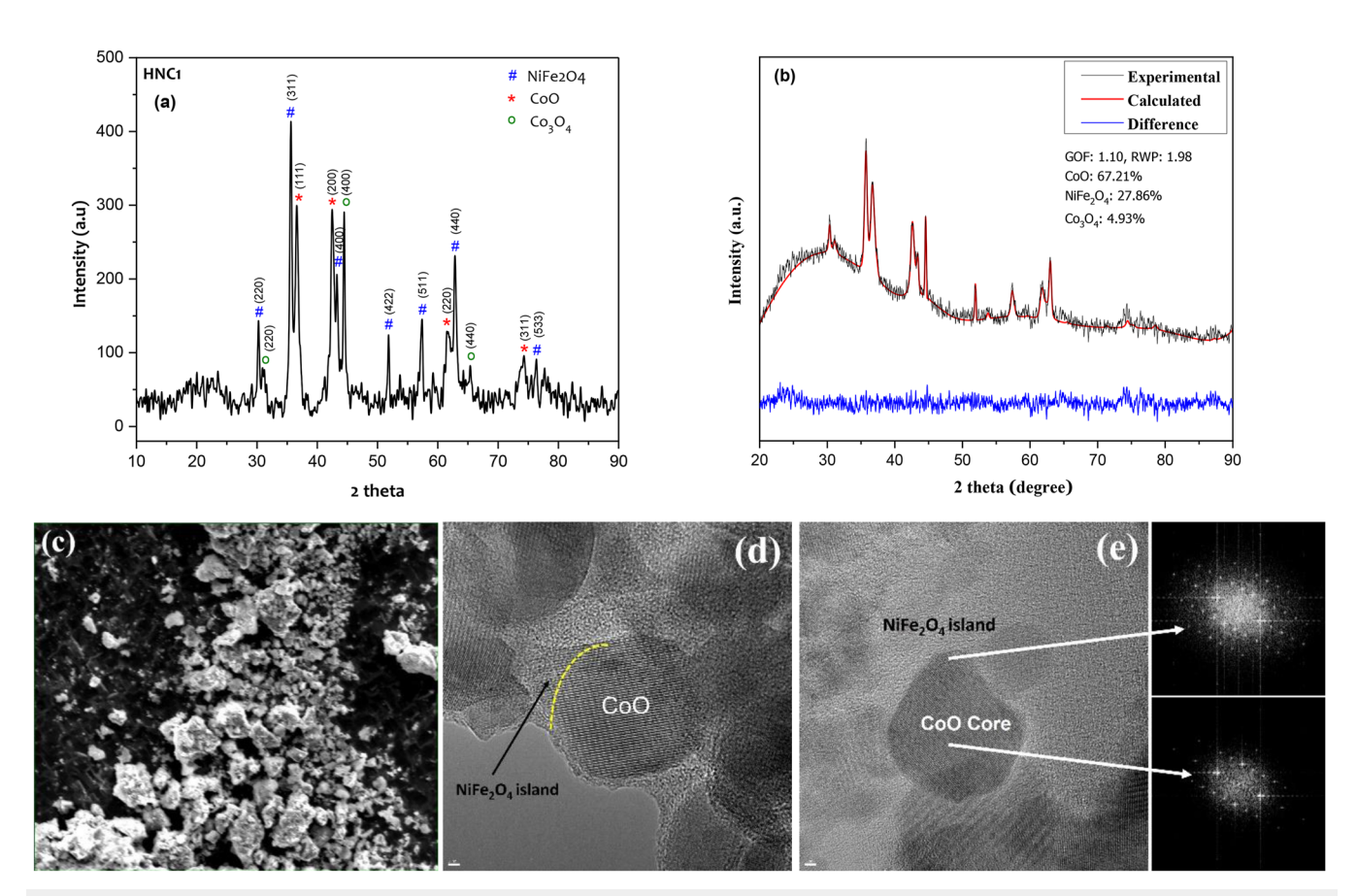


FIG. 1. (a) XRD data collected from the HNC1 sample; (b) Rietveld refinement fitting of the powder XRD pattern of HNC1; (c) An SEM image of the core-overgrowth nanoparticles with scale of 50 μm, (d) An HRTEM image of HNC2 showing topotaxial overgrowth of the NiFe₂O₄ island over the CoO core; (e) An HRTEM image of HNC1 showing core and overgrowth phases along with the respective Fast Fourier Transforms (FFTs).

the presence of Co, as well as Ni, Fe, and O, in the sample. A highresolution TEM (HRTEM) image of an isolated HNC1 nanoparticle is shown in Fig. 1(d). The core and overlayer are separated by an interface that appears to be only slightly more structurally disordered than either the core or overlayer of the isolated HNC, as shown in the TEM image. Our TEM and XRD findings suggest that the overlayer and core regions of the HNCs have identical crystallographic registry, indicating topotaxial growth of the overlayer. Fast Fourier Transforms (FFTs) of the HRTEM images, as shown in Fig. 1(e), support the existence of NiFe₂O₄ nanoislands which are topotaxially formed on the CoO core of the HNC samples. The SEM and TEM images show that both faceted and pseudospherically shaped HNCs are present. The overlayer region of the nanoparticle shown in Fig. 1(d) exhibits nanoisland formation over the core. The HRTEM images collected from the remainder of the samples are consistent with those shown in Fig. 1.

Figure 2(a) shows the low-temperature (5K) magnetization (M) vs magnetic field (H) hysteresis data (M-H loops) for both the FC and ZFC cases. Hysteresis loops for samples HNC1 and HNC3 have the traditional letter "S" shape. However, the loop for HNC2, which has the largest nanocrystallite size, has a tilted-oval type shape.

Table I lists the values of coercivity (H_C), remanent magnetization (M_R), saturation magnetization (M_S), and exchange bias field (H_E) obtained from the hysteresis data for the samples of this investigation at 5 K. The exchange bias (H_E) is derived from the shift of the FC hysteresis loop, relative to the ZFC loop, using the formula $H_E = |(H_{CRight} + H_{Cleft})|/2$, and the coercivity (H_C) is calculated from the ZFC hysteresis loops using the equation, $H_C = |(H_{CRight})|$ $-H_{Cleft}$)/2, where H_{CRight} and H_{Cleft} are the magnetic field values of the ascending and descending parts of the hysteresis loop, respectively, when the magnetization is zero. Notably, we see that all of the samples exhibit highly robust H_C values. In addition, all of the samples possess substantial H_E values. The FiM phase directly affects the saturation magnetization and remanent magnetization values in the HNCs. A higher percentage of FiM overgrowth formation is indicated by higher values of M_S and M_R. Fig. 2(b) shows the exchange bias and coercivity in relation to temperature for the HNC1 sample. We observe that the H_E first increases with an increase in temperature and then progressively drops, whereas the H_C monotonically decreases as the temperature rises. Notably, the H_C is found to persist at 300 K for HNC1, indicating persistence of spin order at room temperature. Due to thermal fluctuations of the uncompensated

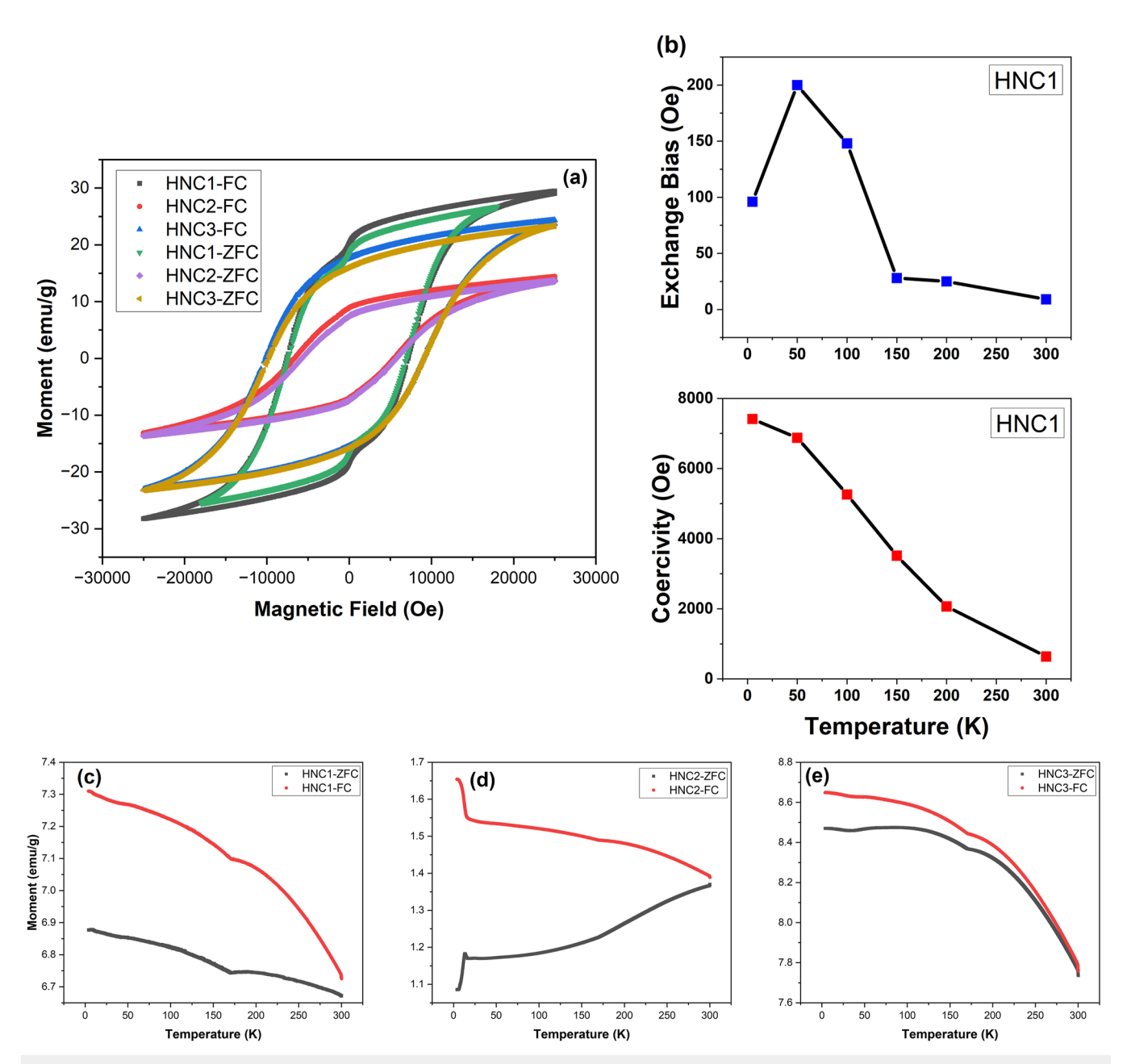


FIG. 2. (a) Magnetization vs applied field (M vs H) data for CoO/NiFe₂O₄ HNCs at 5 K for both zero field cooled (ZFC) and field cooled (FC) measurements; (b) HNC1's exchange bias and coercivity as a function of temperature; (c)–(e) represent the magnetization vs temperature for HNC1, HNC2, and HNC3 sample respectively under ZFC (black lines) and FC (red lines) conditions.

spins at the core/overlayer interface overcoming the AFM anisotropy energy of the CoO core, the exchange bias approaches zero at higher temperatures. Fig. 2(c) shows the FC and ZFC magne tization (M) curves measured from the HNC samples as a function of temperature (T). The ZFC curves generally approach but do not reach a bifurcation point with the FC curves at higher temperatures. Two factors could account for the absence of a bifurcation

temperature: (i) it exceeds 300 K; or (ii) too high of an external field (50 Oe) was applied during the measurement of the M-T curves. Below about 200 K, the ZFC curves for samples HNC1 and HNC3 show two kink-like features that correspond with onsets of rising FC magnetization with decreasing temperature, respectively. For sample HNC2, an additional low-temperature transition is observed near 16 K in both the ZFC and FC curves. We speculate that this

transition may be indicative of spin glass or frustrated/frozen spin behavior.

IV. CONCLUSIONS

In conclusion, we have synthesized for the first-time novel CoO/NiFe₂O₄ HNCs. An AFM CoO nanoparticle core is coated with a FiM NiFe₂O₄ overlayer to form the HNCs using a threestep synthesis process: thermal decomposition for the core and a combination of rotary evaporation and hydrothermal synthesis for core-overgrowth formation. The HRTEM images and data analysis indicate topotaxial growth of the NiFe2O4 spinel overlayer nanophase on the CoO core of the HNCs. The magnetometry data analysis results are consistent with an inverse magnetic AFM/FiM core/overlayer formation for the HNCs. Furthermore, our magnetometry data show that all of the HNC samples exhibit substantial coercivity values whereas the samples having the smaller overall size also have significant exchange bias field values, at 5 K. We find that the coercivity for one of the samples (HNC1) persists at room temperature conditions. This finding demonstrates the potential of our composite nanophase materials for magnetic applications.

SUPPLEMENTARY MATERIAL

See supplementary material for XRD spectra and a size histogram obtained from TEM imaging.

ACKNOWLEDGMENTS

The PPMS measurements were performed at the Cornell Center for Materials Research Shared Facilities, which are supported through the NSF MRSEC program (DMR-1719875).

AUTHOR DECLARATIONS

Conflict of Interest

The authors have no conflicts to disclose.

Author Contributions

Muhammad S. Uddin: Conceptualization (equal); Data curation (lead); Formal analysis (lead); Investigation (lead); Methodology (equal); Project administration (equal); Software (lead); Validation (equal); Visualization (equal); Writing – original draft (lead); Writing – review & editing (equal). **Robert A. Mayanovic**: Concep-

tualization (equal); Data curation (equal); Formal analysis (equal); Funding acquisition (lead); Investigation (equal); Methodology (equal); Project administration (equal); Resources (lead); Software (equal); Supervision (lead); Validation (lead); Visualization (equal); Writing – original draft (equal); Writing – review & editing (lead). Mourad Benamara: Investigation (equal); Resources (equal); Software (equal); Supervision (equal).

DATA AVAILABILITY

The data that support the findings of this study are available within the article.

REFERENCES

- ¹S. Hasan, R. A. Mayanovic, and M. Benamara, AIP Advances 8, 056305 (2018).
- ²R. Scarfiello, C. Nobile, and P. D. Cozzoli, Front. Mater. 3, 56 (2016).
- ³T. M. Freire, W. S. Galvão, R. M. Freire, and P. B. A. Fechine, Complex Magnetic Nanostructures: Synthesis, Assembly and Applications (2017), pp. 83–119.
- ⁴N. Fontaíña Troitiño, B. Rivas-Murias, B. Rodríguez-González, and V. Salgueiriño, Chem. Mater. **26**, 5566 (2014).
- ⁵R. Mariño-Fernández, S. H. Masunaga, N. Fontaíña-Troitiño, M. P. Morales, J. Rivas, and V. Salgueirino, J. Phys. Chem. C 115, 13991 (2011).
- ⁶N. Fontaíña-Troitiño, S. Liébana-Viñas, B. Rodríguez-González, Z.-A. Li, M. Spasova, M. Farle, and V. Salgueiriño, Nano Lett. **14**, 640 (2014).
- ⁷I. Sugiyama, N. Shibata, Z. Wang, S. Kobayashi, T. Yamamoto, and Y. Ikuhara, Nature Nanotechnol. **8**, 266 (2013).
- ⁸W. Kuch, L. I. Chelaru, F. Offi, J. Wang, M. Kotsugi, and J. Kirschner, Nature Mater. 5, 128 (2006).
- ⁹ A. A. Shafe, M. D. Hossain, R. A. Mayanovic, V. Roddatis, and M. Benamara, ACS Appl. Mater. Interfaces 13, 24013 (2021).
- ¹⁰ A. López-Ortega, M. Estrader, G. Salazar-Alvarez, A. G. Roca, and J. Nogués, Physics Reports 553, 1 (2015).
- ¹¹B. Issa, I. M. Obaidat, B. A. Albiss, and Y. Haik, Int. J. Mol. Sci. 14, 21266 (2013).
- ¹² J. Nogués, J. Sort, V. Langlais, V. Skumryev, S. Suriñach, J. S. Muñoz, and M. D. Baró, Physics Reports **422**, 65 (2005).
- ¹³E. Lottini, A. López-Ortega, G. Bertoni, S. Turner, M. Meledina, G. Van Tendeloo, C. de Julián Fernández, and C. Sangregorio, Chem. Mater. 28, 4214 (2016).
- ¹⁴G. Lavorato, E. Winkler, A. Ghirri, E. Lima, D. Peddis, H. E. Troiani, D. Fiorani, E. Agostinelli, D. Rinaldi, and R. D. Zysler, Phys. Rev. B **94**, 054432 (2016).
- ¹⁵P. Mulvaney and L. M. Liz-Marzán, in *Colloid Chemistry I*, edited by M. Antonietti (Springer, Berlin, Heidelberg, 2003), pp. 225–246.
- ¹⁶M. El-Kemary, N. Nagy, and I. El-Mehasseb, Materials Science in Semiconductor Processing 16, 1747 (2013).
- ¹⁷S. Hasan, R. A. Mayanovic, and M. Benamara, MRS Advances 2, 3465 (2017).